Proceedings of

Environmental Science and Technology

(2005)

Volume 2

Edited by

William G. Lyon
Jihua Hong
Ramesh K. Reddy

Proceedings of

Environmental Science and Technology

(2005)

Volume 2

Edited by

William G. Lyon
Jihua Hong
Ramesh K. Reddy

American Science Press, New Orleans, USA

Library of Congress Cataloging-in-Publication Data

Proceedings of Environmental Science and Technology 2005 (II)

Proceedings from the First International Conference on Environmental Science and Technology, held January 23-26, 2005 in New Orleans, Louisiana, USA

Includes bibliographical references
ISBN 0-9768853-5-2

I. Lyon, William G., II. Hong, Jihua.
III. Reddy, Ramesh K.
IV. International Conference on Environmental Science and Technology
(1st : 2005 : New Orleans : Louisiana)

Printed in the United States of America

Email: press@AASci.org
Website: www.AASci.org/press

ISBN 0-9768853-5-2
© 2005 American Science Press

SCIENTIFIC/TECHNICAL COMMITTEE
ICEST2005

TABLE OF CONTENTS

Solid Waste Management

On-site and Off-site Remediation

Landfill

Biotransformation of Pollutants

WETLANDS

Conservation and Geochemical Processes of Wetlands

Wetlands for Wastewater Treatment

SEDIMENTS

Contaminated Sediments

Degradation of Organic Pollutants

Transport and Remediation of Organic Pollutant

MODELING

INTRODUCTION

The First International Conference on Environmental Science and Technology 2005 was held in New Orleans, Louisiana, January 23-26, 2005. The Program included 14 sections, containing 59 sessions with approximately 600 platform and poster presentations.

Authors of the presentations accepted for the program were invited to submit their papers to the Conference Organizing Committee. More than 200 papers were received and then reviewed by the editors, session chairs, and the members of the Scientific/Technical Committee of the conference. Those papers and abstracts accepted for publication were assembled into two volumes.

Sections are arranged basically according to their order listed in the original program except the session entitled *Bio-Assessment and Toxicology*. This exception was made to balance the length of the two volumes.

Proceedings of Environmental Science and Technology 2005 (I) contains the following sections:

- Water Pollution and Water Quality Control
- Air Pollution and Air Quality Control
- Bio-Assessment and Toxicology

Papers of more sections are included in *Proceedings of Environmental Science and Technology 2005 (II)*:

- Land (Soil, Waste Solid) Pollution and Remediation
- Ecosystem Restoration
- Wetlands
- Sediments
- Global Change
- Metals
- Organic Pollutants
- Modeling
- GIS, Statistics, and Remote Sensing
- Society and the Environment
- Environmental Analysis and Measurements

We would like to thank the session chairs, who not only presided over their sessions during the conference, but also contributed their time to review papers, suggesting corrections or directly correcting the papers submitted by the presenters in their sessions.

ISBN 0-9768853-5-2

The Conference was sponsored and organized by the American Academy of Sciences and the Shaw Environmental Group, with financial contributions from the following co-sponsors and supporting organizations:

- CIBA Special Chemicals
- Elsevier
- ENVIRO-Klean Remediation Group, Inc.
- Environmental Record Search
- EnviroMetal Technologies, Inc.
- ESRI, Inc.

William G. Lyon, Ph.D.
American Academy of Sciences

Jihua Hong, Ph.D.
American Academy of Sciences

Ramesh K. Reddy, Ph.D.
University of Florida

LAND (SOIL, SOLID WASTE) POLLUTION AND REMEDIATION

ISBN 0-9768853-5-2

ADVECTION AND DIFFUSION IN UNSATURATED SOILS INFLUENCED BY ADSORPTION, CAPILLARITY AND SUCTION

Peter Schick (Technical University of Berlin, Germany)

ABSTRACT: A Two-Component Model for the saturation-suction relationship (pF-curve) of fine-grained soils is proposed that uses the physical water-binding mechanisms capillarity and adsorption. Standardized soil-mechanics index values are sufficient for its application. Accuracy of class-A predictions of pF-curves, a key property for emission and transport calculations in unsaturated soils, is improved considerably. Results are e.g., capillary pore distribution, characteristic inner surface, and amount of adsored water. Coefficient of permeability of partially saturated soils, as well as diffusion coefficients may be predicted using the same set of parameters used for the pF-curve. Thus, the effect of capillary and adsorptive forces is obvious. If the structure that has formed as a result of sufficient drying is incorporated into the next step, this results in models with aggregates and fissure planes. The advective and diffusive transportation properties of the latter have to be superimposed on the properties of the aggregates.

INTRODUCTION

Transport phenomena in porous media may be explained by advection and diffusion. The physical reason for advection (whereby dissolved matter is passively transported by convective flow of pore fluid) is a pressure or temperature gradient; however, substances spread by diffusion even in resting pore fluids because of the extremely small probability of an unequal matter distribution in comparison to the huge number of uniformly distributed states (2nd fundamental theorem of thermodynamics). Transport phenomena are influenced by interactions between pore water and grain surfaces (adsorption and desorption of water and substances) as well as between pore water and pore gas (evaporation, condensation). Often pollutants will spread only in water or gas, depending on their water solubility and vapor pressure.

MATERIALS AND METHODS

pF-Tests with Cohesive and Granular Soils: The Two-Component Model may be applied to all mineral soils that are not dominated by their organic content. Its biggest advantages are for cohesive soils because of their remarkable inner grain surfaces and, therefore, of their pronounced adsorption effects. Experimental determination of the pF-curve is conducted pointwise by several different tests with different accuracy and testing principles: Pulling mercury column, tensiometer, pressure plate test, filter paper and salt solution. Data collected over 7 orders of magnitude by these methods show noticeable scatter (Fredlund, Rahardjo, 1993; Barbour 1998).

RESULTS AND DISCUSSION

ISBN 0-9768853-5-2

Inner Grain Surface and Adsorption Water. The volume of adsorbed water may be calculated from the thickness of adsorbed water layer d_{wA} and corresponding specific surface O, the latter from the grain size number (fraction A_k of gravel/sand/silt/clay: $A_G/A_S/A_U/A_T$ with medium grain diameter d_k = 11.0/0.35 /0.011/0.001 mm), three different constant grain shape factors $\alpha_{k,i}$ and two index values for the mineralogical composition (Schick, 2002) (eq. 1). Distinction of three grain shapes is sufficient: i=1 for cubical and sperical shaped grains ($\alpha_{k,1}$ = 6), i=2 for platelets of thickness e = 0.1 d ($\alpha_{k,2}$ = 24), i=3 for platelets of thickness e = 0.01 d ($\alpha_{k,3}$ = 204). For the coarse grained part only i = 1 was taken, clay content may be represented by only i = 2 and 3, so 7 addends remain (eq. 2). The index values for mineralogical composition are:

- fraction of clay minerals in total silt $A_{TU} = A_{\text{Clay minerals in silt fraction}}/A_U$
- fraction of montmorillonite in total clay minerals $A_{MT} = A_{\text{Mont.}}/A_{\text{Clay min. total}}$

Grain fractions may be calculated by: $A_{Gr,1} = A_{Gr}$, $A_{S,1} = A_S$, $A_{Si,1} = 100\text{-}A_{TU}$, $A_{Si,2} = A_{TU}*(100\text{-}A_{MT})$, $A_{Si,3} = A_{TU}*A_{MT}$, $A_{Cl,2} = 100\text{-}A_{MT}$, $A_{Cl,3} = A_{MT}$. The empirical equations (3) and (4) may be useful (Schick, 2003):

$$O\left[\frac{cm^2}{g}\right] = O_{Gr} + O_{Sa} + O_{Si} + O_{Cl} = \Sigma\ \frac{\alpha_{k,i}[1]\cdot A_{k,i}[\%]/100}{\frac{d_k[mm]}{10}\cdot \rho_{S,k,i}\left[\frac{g}{cm^3}\right]} \tag{1}$$

$$O = O_{Gr,1} + O_{Sa,1} + O_{Si,1} + O_{Si,2} + O_{Si,3} + O_{Cl,2} + O_{Cl,3} \tag{2}$$

$$A_{TU} = 0.127\cdot \ln\left(I_{P(A<0.4mm)}\right) + 0.729 \tag{3}$$

$$A_{MT} = 0.136\cdot \ln\left(I_{P(A<0.4mm)}\right) + 0.393 \tag{4}$$

Adsorbed water is made up of a few molecules thick hydration water ($d = d_{hyd}$) and water bound ever more loosely as the distance increases ($d = 1/\kappa$) (Mitchell, 1993). A unified value of $d_{wA}(\psi\rightarrow 0) = d_{hyd} + 1/\kappa \approx 4$ nm allows fitting of all test results. Pore spaces are filled with adsorbed water in the saturated state as follows from (5). Usually ψ_{0A} = pF 7 (= 1,000,000 kN/m²) is set for maximum suction (Barbour, 1998). Back-calculated values are about 600,000 kN/m² (Schick, 2003). The Two-Component Model contains a correction function (eq. 6) quite similar to (Fredlund, Xing, 1994) - where it has been used for the whole pF-curve - to force the $S_A(\psi)$-curve (eq. 7) through the point ($S_A = 0$; ψ_{0A}).

$$n_{wA}(\psi = 0) = d_{wA}(\psi = 0)\cdot O\cdot \rho_d \tag{5}$$

$$C_{pA} = 1 - \frac{\ln\left(1 + \frac{\psi}{\psi_{kap}}\right)}{\ln\left(1 + \frac{\psi_{0A}}{\psi_{kap}}\right)} \tag{6}$$

$$S_A(\psi) = C_{pA} \cdot \frac{n_{wA}(\psi = 0)}{n} \tag{7}$$

Capillary Pore Size Distribution and Capillary Water. The capillary water fraction $S_C(\psi) = S - S_A$ is being forced through ($S_C = 0$; ψ_{kap}) by a correction function C_{pC} (eq. 8) and follows from eq. (9). The resulting pF-curves $S(\psi)$ show a sharp bend at $\psi = \psi_{kap} \approx 50{,}000$ kN/m², where capillary water vanishes (Fig. 1, right). Therefore, pF-curves of coarse grained soils end in ($S_C = 0$; ψ_{kap}). Eq. (9) still contains the three free parameters a, m, and q. Parameter a may be calculated using geotechnical index values (Schick, 2003) because it is strictly correlated to the Air-Entry Value AEV (Fig. 1). AEV in turn is dependent on a characteristic maximum pore radius of coarse-grained soils and on liquid and shrinkage limits of fine-grained soils, respectively (eq. 10 and 11).

$$C_{pC} = 1 - \frac{\ln\left(1 + \frac{\psi}{\psi_{kap}}\right)}{\ln(2)} \tag{8}$$

$$S_C(\psi) = \left(1 - S_A(\psi = 0)\right) \cdot C_{pC} \cdot \left(\frac{1}{\ln\left(2.718.. + \left(\frac{\psi}{a}\right)^q\right)}\right)^m \tag{9}$$

$$a = 2 \cdot h_{k,p} \cdot \gamma_w = \frac{0{,}30}{f_{kp} \cdot d_{50}[\mathrm{mm}]} \quad \left[\frac{\mathrm{kN}}{\mathrm{m}^2}\right] \text{ (coarse grained)} \tag{10}$$

$$a = (a_1 - a_2 \cdot w_L) \cdot \exp\left(\frac{(w_L - w_S) \cdot \frac{\rho_S}{\rho_W}}{a_3 \cdot w_L - a_4}\right) \quad \left[\frac{\mathrm{kN}}{\mathrm{m}^2}\right] \text{ (fine-grained)} \tag{11}$$

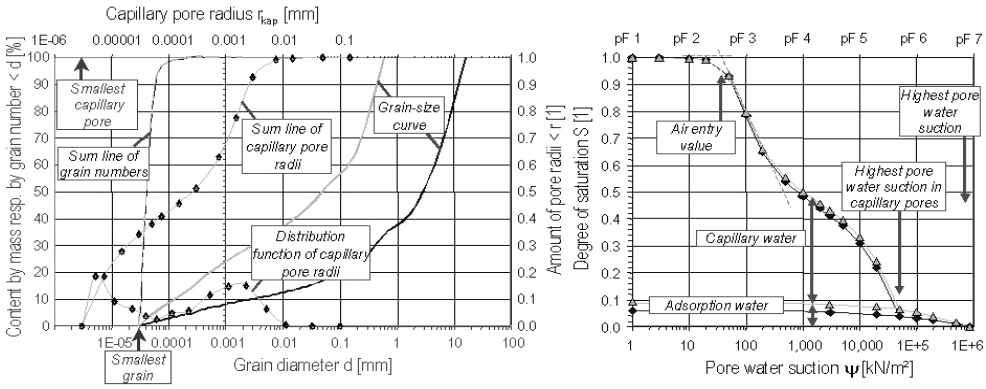

FIGURE 1: Left: Grain-size curves, sum lines and distribution functions of capillary pore radii for two soils, which are only differing in the amount of content < 0,4 mm. Right: pF-curves of both soils according to the Two-Component Model with limit values and water components [Schick, 2003]

Application of Two-Component Model and Required Inputs. Knowing some experimental points of the pF-curve (Fig. 1, right) and the standardized index values of the soil, parameter a follows from (10) or (11), and the pF-curve is already well described after postulating some reliable physical values (Tab. 1). Total porosity or dry density is needed as a state parameter. The nearly inversely proportional parameters m and q are found starting from m [1] = 1 and q [1] = 1; they control the form of the capillary pore radius distribution (Fig. 1, left side). Indeed, if one has to model drying-wetting cycles, a second state parameter S_0 has to be set, and a, m, and q will change during the first cycle.

TABLE 1: Necessary values for application of the Two-Component Model

Name	Needed for calculation of …	Example			
Physical values and constants		**For all soils**			
Surface tension of water	Maximum capillary water suction	T_W = 7.5E-08 kN/mm			
Density of water	Water content and degree of saturation	ρ_W = 1.000 g/cm³			
Smallest radius of capillary pores	Maximum capillary water suction	min r_{kap} = 3E-06 mm			
Wetting angle water - mineral	Capillary water suction	α = 0°			
Thickness of adsorption water layer	Adsorptive bound water fraction	d_{wA} = 4 nm (up to 10...20 nm at high montmorillonite content and high porosity)			
Maximum water suction at S→0	Correction function C_{pA}	ψ_{0A} = 700,000 kN/m² (600,000 .. 1,000,000)			
Classification values		**Soil i**		**Soil i+1**	
Grain size index (or grain size curves)	Specific surface O resp. grain-number line	$A_G/A_S/A_U/A_T$ [%]			
Density of grains	Specific surface O resp. grain-number line	ρ_S [g/cm³]			
Cohesive soils: liquid limit, shrinkage limit, grain density; Non-cohesive soils: Average grain size	Parameter a resp. AEV value	w_L [%] w_S [%], ρ_S [g/cm³], d_{50} [mm]			
Mass fractions: clay minerals / silt grains; montmorillonite / total clay minerals	Specific surface O resp. grain-number line	A_{TU} [%], A_{MT} [%].			
Plasticity index	Estimation of A_{TU} and A_{MT} if no tests available	I_P [%]			
State parameters		**State i_j**	**State i_k**	**...**	**...**
Porosity	Influences adsorptive bound water fraction	n [%]			
Maximum degree of saturation after rewetting	Starting point of hysteresis loops for drying-wetting cycles	S_0 [%]			

Water Permeability and Advective Transport in Unsaturated Soils. The permeability of many soil types may be calculated by (12), e.g. for the <0,4mm-content of "Bentokies" (mixed-grained sealing material, mixed-in-plant, sandy

gravel with clay powders). Reference values ($n^*=n_{100}$; $k^*=k_{100}$ with $\sigma'_V=100kN/m^2$) depend on plasticity. Often parameters m_k = 1.5...2.5, are influenced by many factors. Eq. (12) holds for mechanical one-dimensional compression. Dewatering has similar effects, so (12) may be used for unsaturated soils in the case of $S>>S_A$. If only capillary water participates in the water flow, eq. (13) follows, and $k\rightarrow 0$ for $S\rightarrow S_A$, $k_{100}=k(S=1)$. A pF-curve and eq. (13) is shown in Fig. 2. As water saturation decreases, air saturation increases. Advection of gas may be calculated as Darcy-like pore air flow, accounting for gas concentration, specific weight and viscosity of the pore air.

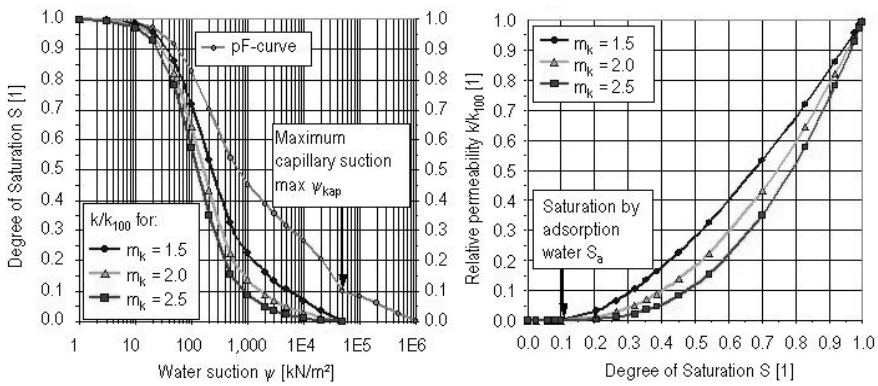

FIGURE 2: Left: pF-curve and relative permeability of unsaturated soil; Right: Relative permeability and degree of saturation acc. to eq. (13) [Schick, 2003]

$$\log\left(\frac{k}{k^*}\right) = m_k \cdot \log\left(\frac{n}{n^*}\right) \tag{12}$$

$$\frac{k}{k_{100}} = \left(S_C^*\right)^{m_k} = \left(\frac{S_C}{\max S_C}\right)^{m_k} \tag{13}$$

Diffusion in Unsaturated Soils. In low permeable soils, an effective diffusion coefficient D_{eff} accounts for the winding pathway of substances by means of a tortuosity factor, τ. A retardation factor 1/R handles ad- and de-sorption on characteristic grain surface areas. Transport equations should account for advective and diffusive transport, degradation, ad- and de-sorption. Neglecting hydraulic gradient and degradation and setting $n \neq f(x,t)$, $R \neq f(t)$, $d_0 \neq f(x)$, $\tau \neq f(x)$ leads to (14). For all cases with low sorption (1/R=1), e.g. chloride in water or tetrachloroethene in gas, the tortuosity factor is the ratio D_{eff}/d_0, which decreases with porosity (Schick, Wunsch, 1994) (Fig. 3). As in Fig. 2 right, a decreasing diffusion coefficient has been observed with lower saturation (Barbour, 1998). There is diffusion in the adsorbed water layer up to S = 0, but the free diffusion coefficient d_0 becomes very small since it is inversely proportional to viscosity η_w of water according to the Stokes-Einstein equation (Atkins, 1993). Replacing the viscosity of water by the equivalent term from Rate Process Theory (Schick, 2003) gives eq. (15) (where r_h [L]: equivalent radius of particle; λ [L]: length of energy barrier, h: Plancks constant; $\Delta F/R_GT$ [1]: relative activation

energy barrier, R_G: Gas constant, T: Absolute temperature, N_A: Avogadros No.). Free diffusion in adsorption water gets smaller due to increasing activation energy approaching the clay-mineral grain surface. Eq. (16) results if total diffusion coefficient $D_{eff}(S)$ for water-solved substances is summable from the capillary water part and the adsorbed water part.

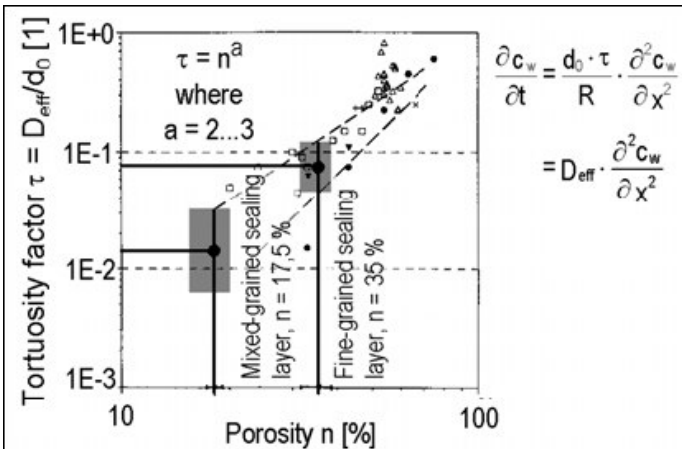

FIGURE 3: Tortuosity factor of chloride ions in soils (Schick, Wunsch, 1994)

$$\frac{\partial c_w}{\partial t} = \frac{d_0 \cdot \tau}{R} \cdot \frac{\partial^2 c_w}{\partial x^2} = D_{eff} \cdot \frac{\partial^2 c_w}{\partial x^2} \tag{14}$$

$$d_0 = \frac{R_G \cdot T}{f \cdot \eta_w} = \frac{R_G \cdot T}{6 \cdot \pi \cdot r_h \cdot \eta_w} = \frac{R_G \cdot T \cdot \lambda^3}{6 \cdot \pi \cdot r_h \cdot h \cdot \exp\left(\frac{\Delta F}{R \cdot T}\right) \cdot N_A} \tag{15}$$

$$\frac{D_{eff}(S)}{D_{eff}(S=1)} = S_C \cdot \frac{d_{0,C} \cdot \tau_C(S)}{R \cdot D_{eff}(S=1)} + S_A \cdot \frac{d_{0,A} \cdot \tau_A(S)}{R \cdot D_{eff}(S=1)} \tag{16}$$

CONCLUSIONS.

The Two-Component Model enables evaluation of the pF-curve with common, meaningful geotechnical and physical parameters. It gives information about the amount of adsorbed water, the characteristic inner grain surface and capillary pore-size distribution, which may be used for improved investigation of transport parameters in partially saturated soils. The distinction between water bound by capillary and adsorptive forces in the Two-Component Model is adequate and sufficient in this respect. Saturation-dependent concentration profiles were calculated for the homogenous and steady cases. Using the Peclet Number it can be shown, that ion transportation becomes more diffusion-controlled as water saturation vanishes.

Current research deals with application of the Two-Component Model on structuring of fine-grained soils (e.g. Schick, Schmitz, 2004), a wide-spread near-

surface phenomenon with impacts on environmental soil problems and on safety of geotechnical constructions. During drying-wetting cycles, structuring in soils will always appear and will change the transport mechanisms and strength dramatically. Nevertheless, the corresponding shrunken and cracked state is still difficult to predict. By using the Two-Component Model, some improvements are expected in this field of unsaturated soil mechanics.

ACKNOWLEDGEMENTS

This research was supported by the Federal Republic of Germany and is continued presently granted by the German DFG.

REFERENCES

Atkins, P.W. 1993. *Kurzlehrbuch physikalische Chemie* (Textbook physical chemistry). Spektrum Verlag, Heidelberg.

Barbour 1998. The soil-water characteristic curve: a historical perspective. 19th Canadian Geotechnical Colloquium, *Can. Geotech. J.* 35, 873-894.

Fredlund, Rahardjo 1993. Soil Mech. for Unsaturated Soils. Wiley, New York.

Fredlund, Xing 1994. Equations for the soil-water characteristic curve. *Can. Geotech. J* 31: 521-532 (1994).

Mitchell, J.K. 1993. *Fundamentals of Soil Behaviour*. 2nd Ed., Wiley, N.Y.

Schick, P. 1997: Bodenmechanische und bautechnische Eigenschaften von Bentokiesdichtungen (Properties of Bentokies liners for waste deposits – proof of security and serviceability). *Bautechnik* 74, H.5, S.320-330.

Schick, P. 2002. Anwendung eines Zwei-Komponenten-Modells der pF-Kurve auf Strukturänderungen in Böden (Application of a Two-Component Model of the pF-curve to structure changes in soils). *Bautechnik* 79 (2002), Heft 2.

Schick, P. 2003. Ein quantitatives Zwei-Komponenten-Modell der Porenwas-ser-Bindekräfte in teilgesättigten Böden. Mitt. Inst. Bodenmech. u. Grund-bau, UniBwM, H. 17, 2003, im Druck (A quantitative Two-Component Model of the water-binding forces in partially saturated soils, in print).

Schick, P. 2003. The pF-curve of fine-grained soils at high pore water suction. Int. Conf. "From exp. evidence towards num. modelling unsaturated soils", ISSMGE, Sept.18-19,2003, Bauhaus-Univ. Weimar, Germany, Springer.

Schick, P., Schmitz, S.M. 2004. X-Ray Tomography of Structures in Clay Geosynthetic Barriers (CBR-C). In: Floss et al (eds.): EuroGeo3 Geosynthetics Conf., March 01-03 2004, Munich, Germany.

Schick, P., Wunsch, R. 1994. Diffusion chlorierter Kohlenwasserstoffe durch Bentokiesdichtungen (Diffusion of chlorinated hydrocarbons through Bentokies liners). *Geotechnik* 18, S.197-204.

FATE OF *ESCHERICHIA COLI* O157:H7 IN IRRIGATION WATER ON SOILS AND PLANTS

A. Mark Ibekwe, Pamela M. Watt, Peter J. Shouse, and Catherine M. Grieve
USDA-ARS, George E. Brown Jr. Salinity Lab Riverside, CA 92507

ABSTRACT: A real-time PCR method was developed to detect and quantify *Escherichia coli* O157:H7/pGFP *(E. coli*). A probe was designed to hybridize with the *eae* gene of *E. coli* O157:H7. The probe was incorporated into real-time PCR containing DNA extracted from the phyllosphere, rhizosphere, and non-rhizosphere soils irrigated with water artificially contaminated with *E.coli* O157:H7. The detection limit for *E. coli* O157:H7 from quantification by real-time PCR was 1.4 x 10^3 in rhizoshere and phyllosphere samples. *E. coli* O157:H7 concentrations were higher in the rhizosphere than in the non-rhizosphere soils and leaf surfaces, and persisted longer in clay soil. The concentrations of *E. coli* O157:H7 obtained by real-time PCR were comparable to the concentrations obtained by traditional culture methods during the first three days of inoculation, and thereafter, the concentrations by real-time PCR were higher. The persistence of *E. coli* O157:H7 in phyllosphere, rhizosphere, and non-rhizosphere soils over 45 days may play a significant part in the re-contamination cycle of produce in the environment. Therefore, the rapidity and the feasibility of the assay may be a useful tool for quantification and monitoring of *E. coli* O157:H7 in irrigation water and contaminated fresh produce.

INTRODUCTION

Contaminated irrigation water is one of the most common vehicles by which *E. coli* O157:H7 may be introduced into crops. *Escherichia coli* O157:H7 causes a wide spectrum of diseases in humans, ranging from mild to bloody diarrhea, hemorrhagic colitis, and complications, including hemolytic uremic syndrome (HUS) and seizures that are particularly severe in children (Franke et al., 1995). Recently, Solomon et al., 2002 demonstrated the transmission of *E. coli* O157:H7 from manure-contaminated soil and irrigation water to lettuce plants using laser scanning confocal microscopy, epifluorescence microscopy and recovery of viable cells from the inner tissues of plants. They attributed the presence of *E. coli* O157:H7 in the edible portion of the plant to the direct migration through the conducting tissues of the root system.

Little research has been done on the quantification of this pathogen in the rhizosphere and phyllosphere of plants. The recent availability of new technologies such as real-time PCR has greatly aided the study of pathogens such as *E .coli* O157:H7 in the environment (Oberst et al., 1998). Recently, Ibekwe et al., 2002 described quantification of *E. coli* O157:H7 in soil, cattle feces, manure, and waste water using multiplex real-time PCR for quantification of natural *E. coli* O157:H7 from these samples. The purpose of this study was to use real-time PCR to determine the persistence of *E. coli* O157:H7 from contaminated irrigation water in the rhizosphere and phyllosphere of lettuce grown under flood

ISBN 0-9768853-5-2

irrigation system and to compare these results with culture method based on the enumeration of pGFP expressing *E. coli* O157:H7.

MATERIALS AND METHODS

Bacterial strains, growth conditions, and inoculum preparation. The *E. coli* O157:H7 strain 34 with green fluorescent protein (pGFP) was used for this study. Plasmid construction of the strain has previously been described (Fratamico *et al.,* 1997). *E. coli* O157:H7/pGFP was cultured at 37 ^{o}C overnight in modified Tryptic Soy broth (mTSB)(Difco Laboratories Inc., Cockeysville, MD) supplemented with 100 µg of ampicillin mL^{-1} (Sigma, St Louis, MO). Cells were harvested by centrifugation at 3500 g for 10 min and resuspended in PBS (Fisher Scientific, Pittsburgh, PA) to a concentration of ~10^8 CFU mL^{-1}.

Soil, preparation of irrigation water and plants, and recovery of *E. coli* O157:H7/pGFP. Clay soil and sandy soil were collected from Mystic Lake dry bed and the Santa Ana River bed, respectively for this study. The soils were processed as described by Ibekwe and Grieve, 2004. Soils were tested by culture and PCR methods to make sure that they are *E. coli* O157:H7 negative. Seeds of green romaine lettuce *Lactuca sativa* (*L.*) cv. Green Forest) were grown in two growth chambers at 20 °C with 70% relative humidity and a photoperiod consisting of 16 h of light and 8 h of darkness.

The experiment was a completely randomized design with three replications. There were ten plants in each tray at transplanting, and one plant was harvested from each tray during analysis as stated below. The first irrigation with contaminated water containing *E. coli* O157:H7(pGFP) occurred at transplanting (day 1) for both soils, and the second contamination event occurred 15 days later. Irrigation solutions were prepared in 1000 L reservoirs and pumped to provide irrigation to the clay and sandy soil in polypropylene trays. A one liter solution containing ~ 10^7 *E. coli* O157:H7/pGFP with 100 µg of ampicillin ml^{-1} was applied directly to the irrigation lines and delivered to each tray with four drip lines.

Plant phyllosphere and rhizosphere soil samples were aseptically sampled for analysis at 3, 5, 9, 12, 15, 18, 25, 29, and 45 days after transplantation. Phyllosphere and rhizosphere samples were separated by cutting the above ground part of the plant into different sterile Petri dishes or collection bags and treating the rhizhosphere the same. Samples were processed immediately in the laboratory. Bacteria were recovered from the phyllosphere (leaf surface) by homogenization with 100 mL of PBS for 2 min at 260 rpm in a Seward Stomacher 400 Circulator (Seward Ltd., London, UK). The same procedure was used to recover bacteria from the rhizosphere (volume of soil adjacent to and tightly held by plant roots and influenced by the plant roots). The homogenate was centrifuged at 3000 g for 10 min, the pellet was resuspended in 2 mL of PBS, 100 µL plated on mTSA with ampicillin and incubated at 37 ^{o}C overnight. *E. coli* O157:H7/pGFP colonies were enumerated under a hand-held Spectroline ultra-violet lamp (Spectronics Corporation, Westbury, NY). Portions of the concentrated samples from

rhizosphere and phyllosphere samples were used for extraction of total bacterial DNA and the DNA was used for quantification of *E. coli* O157:H7 by real-time PCR.

DNA extraction and Primer and probe design for real-time PCR. For the constructions of standard curves for real-time PCR, genomic DNA was extracted from pure culture of *E. coli* O157:H7/pGFP, grown for 8 h at 37 ^{o}C and extracted with the Qiagen tissue kit (QIAamp DNA Mini Kit; Valencia, CA). The standard curves from O157:H7/pGFP was used for the determination of detection limits of the *E. coli* by real-time PCR. Total bacterial DNA was extracted from rhizosphere and phyllosphere samples with the Ultra Clean Soil DNA Kit (MoBio Laboratories, Solana Beach, CA) and stored at –20° C. Primers and probe used for the detection and quantification of the *eae* gene in *E. coli* O157:H7 was as described by Ibekwe *et al.,* (2002). Real-time, quantitative PCR was performed with the iCycler iQ Real-Time PCR as described by Ibekwe et al., 2002.

Standard curves generated from plotting the threshold cycle (C_T) versus $\log_{10}$ of starting DNA quantities (pg) were used for determining the detection limit of the assay. The standard curve was constructed from known quantities of genomic DNA extracted from *E. coli* O157: H7. The titers (CFU mL^{-1}) of *E. coli* O157:H7 present in unknown samples were determined from the standard curve. The slopes of the standard curves were calculated by performing linear regression analysis within the iCycler iQ software to compare the PCR amplification efficiency and detection sensitivity among different experiments. Amplification efficiency (E) was estimated by using the slope of the standard curve and the formula: $E = (10^{-1/slope})-1$. Reaction with 100% efficiency generated a slope of –3.32. Standardization of DNA quantities between known and unknown samples was accomplished by dividing total CFU mL^{-1} of *E. coli* O157:H7/pGFP by the mean starting DNA concentration of that CFU mL^{-1} from the instrument analysis as described previously (Ibekwe et al., 2002). This resulted in a CFU mL^{-1} index, which was used as a multiplier to calculate the CFU mL^{-1} of all unknown samples. The CFU mL^{-1} index was obtained from the highest DNA quantity to estimate CFU mL^{-1} from lower DNA quantities.

RESULTS AND DISCUSSION

Sensitivity, standard curve, and amplification efficiency of real-time PCR assay. Previous work (Ibekwe *et al.,* 2002) showed the *eae* gene to be a much conserved marker for distinguishing *E. coli* O157:H7 from other serotypes of *E. coli* after analyzing 33 Shiga toxigenic *E. coli* (STEC) and non-STEC *E. coli* strains. The sensitivity of the Texas Red-labeled probe to specifically detect and quantify the *eae* gene was determined by plotting the log DNA starting quantities of *E. coli* O157:H7/pGFP. The mean C_T values were between 21 and 23 when 5 to 10 pg DNA mL^{-1} was used as a template. The dynamic range for cell detection of the quantitative real-time PCR was determined to be between 10^3 to 10^8 CFU mL^{-1} of *E. coli* pGFP (data not shown). Concentrations of *E. coli* O157:H7 in plant and soil samples were calculated from this standard curve. Based on this

approach, a correlation was observed between the C_T and the CFU mL^{-1} of the starting quantity of *E. coli* O157:H7 DNA, with a detection limit of 1.4 X 10^3 CFU mL^{-1} with a correlation coefficient of about 0.99 for each curve.

Fate of *E. coli* O157:H7 in phyllosphere and rhizosphere as determined by plate count of pGFP colonies and real-time PCR. *E. coli* O157:H7 populations in the phyllosphere samples after the first contamination event decreased an average > 3 logs between day 3 and 12 in the clay soil and < 4 logs for the sandy soil (Fig. 1a). On the average, about 170 CFU of *E. coli* O157:H7 g^{-1} was recovered from lettuce phyllosphere

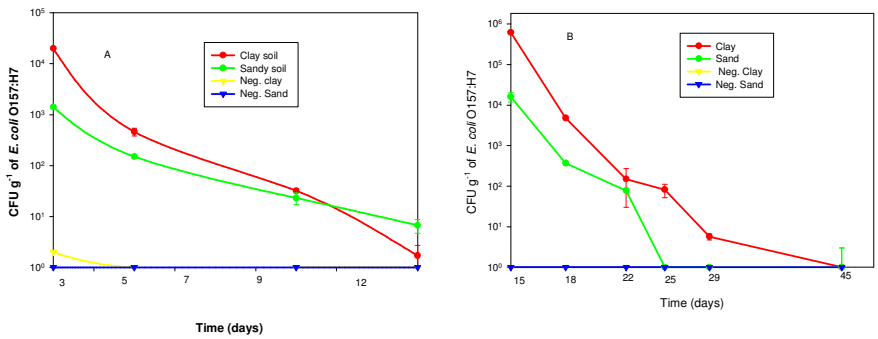

Fig. 1. Quantification of *E. coli* O157:H7 in the phyllosphere after (a) 12 d and (b) from day 15 to 45. *E. coli* O157:H7 enumerated from clay and sandy soils by plate count of pGFP.

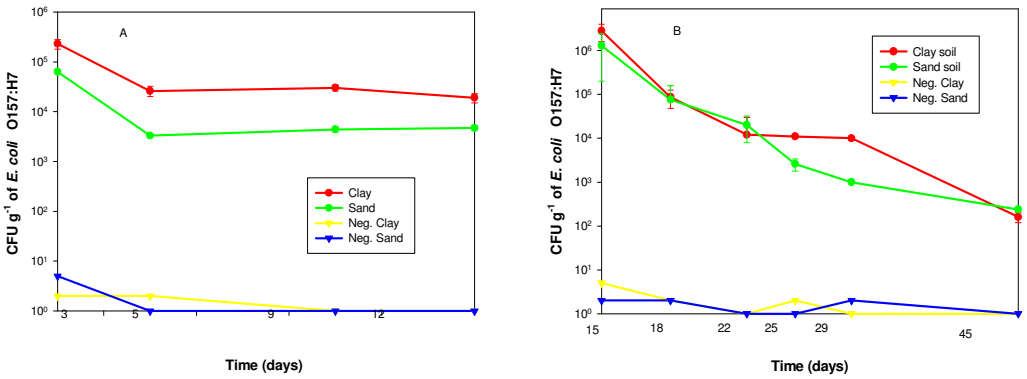

Fig. 2. Quantification of *E. coli* O157:H7 in the rhizosphere after (a) 12 d and (b) from day 15 to 45. *E. coli* O157:H7 enumerated from clay and sandy soils by plate count of pGFP.

grown on clay soil and about 67 CFU of *E. coli* O157:H7 g^{-1} was recovered from lettuce phyllosphere grown on sandy soil after the first 12 days. Following the

second contamination event, the concentration of the pathogen in the phyllosphere of both soils after 45 days dropped to ≤ 10 CFU g^{-1} (Fig. 1b). Throughout the 45 days study, the *E. coli* O157:H7 population decline was linear in the phyllosphere. The concentration of *E. coli* O157:H7/pGFP in rhizosphere soils was 10^5 CFU g^{-1} in both soils at day 12 (Fig. 2a), with the clay soil significantly higher than the sandy soil. However, the trend in survival after the second contamination event (from day 15 to 45) was significantly different from the first contamination event (Fig 2b). There were no differences in the concentrations between the two soils by the end of the study. The survival of *E. coli* O157:H7/pGFP in the rhizosphere was 2 logs higher in the rhizosphere than in the leaves of the plants. Furthermore, the *E. coli* O157:H7/pGFP population decline rate constant was significantly different on both the clay and sandy soils (r^2 = 0.99 and P = 0.001). Thus *E. coli* O157:H7/pGFP survived best and remained culturable for a longer period of time in the rhizosphere. This agreed with a recent report by Gagliardi and Karns (2000), that *E. coli* O157:H7 persistence was enhanced in the rhizosphere of rye and legumes grown in clay soil.

Table 1. Quantification of *E. coli* O157:H7 by real-time PCR during the first and the second inoculation events

Soil type	Day	Sample type	Real-time PCR of *eae* gene (CFU g^{-1})*	Soil type	Day	Sample type	Real-time PCR for *eae* gene (CFU g^{-1})*
Clay	3	Phyllosphere	$1.1 \times 10^5 \pm 6.0 \times 10^5$	Clay	15	Phyllosphere	$7.0 \times 10^6 \pm 8.1 \times 10^6$
		Rhizosphere	$2.5 \times 10^6 \pm 2.1 \times 10^5$			Rhizosphere	$1.7 \times 10^6 \pm 1.6 \times 10^6$
	5	Phyllosphere	$4.9 \times 10^3 \pm 6.7 \times 10^3$		18	Phyllosphere	$3.2 \times 10^5 \pm 4.5 \times 10^5$
		Rhizosphere	$1.5 \times 10^5 \pm 2.5 \times 10^4$			Rhizosphere	$2.5 \times 10^6 \pm 1.2 \times 10^5$
	9	Phyllosphere	$1.4 \times 10^3 \pm 3.4 \times 10^3$		22	Phyllosphere	$3.6 \times 10^5 \pm 3.2 \times 10^5$
		Rhizosphere	$1.7 \times 10^5 \pm 1.6 \times 10^5$			Rhizosphere	$1.1 \times 10^6 \pm 9.3 \times 10^5$
	12	Phyllosphere	$1.1 \times 10^3 \pm 6.9 \times 10^2$		25	Phyllosphere	$6.6 \times 10^4 \pm 3.2 \times 10^4$
		Rhizosphere	$1.4 \times 10^5 \pm 2.1 \times 10^5$			Rhizosphere	$6.9 \times 10^5 \pm 4.0 \times 10^5$
Sand	3	Phyllosphere	$5.9 \times 10^5 \pm 2.9 \times 10^5$		29	Phyllosphere	$3.6 \times 10^3 \pm 1.8 \times 10^3$
		Rhizosphere	$2.5 \times 10^5 \pm 1.5 \times 10^5$			Rhizosphere	$2.0 \times 10^5 \pm 2.5 \times 10^5$
	5	Phyllosphere	$3.2 \times 10^4 \pm 1.9 \times 10^4$		45	Phyllosphere	$1.7 \times 10^3 \pm 7.9 \times 10^2$
		Rhizosphere	$7.1 \times 10^5 \pm 9.4 \times 10^5$			Rhizosphere	$9.8 \times 10^4 \pm 4.2 \times 10^4$
	9	Phyllosphere	$1.3 \times 10^3 \pm 1.7 \times 10^3$	Sand	15	Phyllosphere	$2.1 \times 10^5 \pm 1.6 \times 10^5$
		Rhizosphere	$3.8 \times 10^4 \pm 4.4 \times 10^4$			Rhizosphere	$3.0 \times 10^6 \pm 2.6 \times 10^6$
	12	Phyllosphere	$2.4 \times 10^3 \pm 1.4 \times 10^3$		18	Phyllosphere	$6.1 \times 10^4 \pm 3.8 \times 10^4$
		Rhizosphere	$3.6 \times 10^3 \pm 3.7 \times 10^3$			Rhizosphere	$4.1 \times 10^6 \pm 6.5 \times 10^6$
					22	Phyllosphere	$2.3 \times 10^3 \pm 1.6 \times 10^3$
						Rhizosphere	$6.7 \times 10^5 \pm 5.9 \times 10^5$
					25	Phyllosphere	$4.5 \times 10^2 \pm 7.9 \times 10^1$
						Rhizosphere	$4.3 \times 10^4 \pm 3.7 \times 10^4$
					29	Phyllosphere	$2.4 \times 10^2 \pm 6.6 \times 10^2$
						Rhizosphere	$1.8 \times 10^4 \pm 1.9 \times 10^3$
					45	Phyllosphere	$5.2 \times 10^2 \pm 2.6 \times 10^2$
						Rhizosphere	$1.4 \times 10^3 \pm 1.4 \times 10^3$

*The numbers presented are means and standard deviation of triplicate samples.

Quantitative real-time PCR analysis of these samples revealed linearity between the C_T values and the starting quantities of DNA representing 10^3 to 10^8 CFU g^{-1}. Amplification efficiencies and the goodness of fit analysis for the standard curves were higher than 99%. Table 1 shows the quantification of *E. coli* O157:H7/pGFP detected over several weeks in the phyllosphere and rhizosphere soil samples by real-time PCR. The concentrations of *E. coli* O157:H7 in the rhizosphere soils obtained by real-time PCR were very close to the numbers of

pGFP colonies obtained by the traditional culture methods on mTSA during the first three to five days of the first contamination event, and days 15 to 18 of the second contamination event. After this point, except in a few instances, the concentration by real-time PCR was higher by 1 to 3 logs. This was observed in clay soil in day 9, sand rhizosphere day 9, and 15. Our study shows that pGFP is highly stable for a few days, but it may not be a good marker for monitoring long term survival of bacteria. The higher concentrations of bacteria determined by real-time PCR versus plate count, 9 days after inoculation in some instances, confirmed this observation.

The ability to quantify *E. coli* O157:H7 in fresh produce and other food matrices without using culture methods will be very helpful for developing risk assessment models. Currently, most data demonstrating the risk of *E. coli* O157:H7 in food depend on culture techniques (Duffy and Schaffner, 2001). Our study suggests that *E. coli* O157:H7 has the capability to exploit the nutrient resources on leaves under conditions in which the physical environment does not limit their activities, and therefore can survive in large numbers as part of the community. This observation was confirmed in a related study by Ibekwe and Grieve, 2004, which showed that microbial community development in lettuce, took about 7 to 12 days and that this may be the most likely period for maximum pathogen contamination in plants**.** The automated PCR amplification and detection of target gene amplicons described in this study is conducive for screening large numbers of samples in a single assay. The real-time PCR can be a useful method for processing plants to monitor the contamination of fresh produce for risk analysis before sending produce to the consumers.

REFERENCES

Duffy, S. and Schaffner, D. W. 2001. Modeling the survival of *Escherichia coli* O157:H7 in apple cider using probability distribution functions for quantitative risk assessment. J. Food Protect. **64**:599–605.

Franke, S., Harmsen, D., Caprioli, A., Pierard, D., Wieler, L. H.and Karch, H. 1995. Clonal relatedness of Shiga-like toxin-producing *Escherichia coli* O101 of human and porcine origin. J. Clin. Microbiol. **33**: 3174-3178.

Fratamico, P.M., Deng, M.Y., Strobaugh,T.P., and Palumbo, S.A. 1997. Construction and characterization of *Escherichia coli* O157: H7 Strains expressing firefly luciferase and green fluorescent protein and their use in survival studies. J Food Prot. **60**: 1167-1173.

Gagliardi, J. V. and Karns, J. S. 2000. Leaching of *Escherichia coli* O157:H7 in diverse soils under various agricultural management practices. Appl. Environ. Microbiol. **66:** 877-883.

Ibekwe, A. M., Watt, P. M., Grieve, C. M., Sharma, V. K. and Lyons, S. R. 2002. Multiplex fluorogenic real-time PCR for detection and quantification of *Escherichia coli* O157:H7 in dairy wastewater wetlands. Appl. Environ. Microbiol. **68**: 4853-4862.

Ibekwe, A. M., and Grieve, C. M. 2004. Changes in developing plant microbial community structure as affected by contaminated water. FEMS Microbiol. Ecol. **48**: 239–248

Oberst, R. D., Hays, M. P., Bohra, L. K., Phebus, R. K., Yamashiro, C. T., Paszko-Kolva, C., Flood, S. J. A., Sargeant, J. M. and Gellespie. J. R. 1998. PCR-based DNA amplification and presumptive detection of *Escherichia coli* O157:H7 with internal fluorogenic probe and the 5' nuclease (TaqMan) assay. Appl. Environ. Microbiol. **64**: 3389-3396.

Solomon, E. B., Yaron, S. and Matthews K. R. 2002. Transmission of *Escherichia coli* O157:H7 from contaminated manure and irrigation water to lettuce plant tissue and its subsequent internalization. Appl. Environ. Microbiol. **68**, 397-400.

INNOVATIVE CHARACTERIZATION OF MULTI-COMPONENT DNAPL IN A HETEROGENEOUS AQUIFER

Ed Meyers. Lewis Davies, Nicole Scroggins, and Jason Perdicaris
(Earth Tech, Orlando, Florida)
Brad Goeb (Universal City Property Management, Orlando, Florida)

ABSTRACT: Recent groundwater assessment activities at a former unlined industrial landfill have delineated a 5-acre dissolved-phase groundwater plume, extending to a depth of 150 feet below land surface (bls). Dissolved-phase concentrations in excess of ten-percent solubility were detected for several contaminants, providing presumptive evidence that non-aqueous phase liquids (NAPLs) may be present at the site. NAPL distribution in the subsurface is typically localized; therefore, obtaining direct evidence of NAPL is often difficult. Conventional NAPL investigations typically involve time-consuming continuous soil borings and extensive soil and groundwater sampling to determine NAPL distribution. As an alternative to conventional methods, a Membrane Interface Probe (MIP) equipped with a soil conductivity detector was used to obtain real-time qualitative contaminant distribution and geophysical data, which assisted in determining the subsurface distribution of NAPL. Although preliminary groundwater analytical data indicated the potential for NAPL to exist throughout a large area of the plume, MIP investigation results and subsequent soil sampling indicate that the NAPL source area is smaller and more localized than groundwater solubility data suggests. The data obtained during the MIP investigation will reduce the time and cost of site remediation by focusing remedial actions on a smaller source area.